Electrochimica Acta 400 (2021) 139413

Contents lists available at ScienceDirect

Electrochimica Acta

journal homepage: www.elsevier.com/locate/electacta

Criterion for finding the optimal electrocatalyst at any overpotential

Yufan Zhang[a,b], Jun Huang[a], Michael Eikerling[a,b,*]

[a] Theory and Computation of Energy Materials (IEK-13), Institute of Energy and Climate Research, Forschungszentrum Jülich GmbH, 52425 Jülich, Germany
[b] Chair of Theory and Computation of Energy Materials, Faculty of Georesources and Materials Engineering, RWTH Aachen University, 52062 Aachen, Germany

ARTICLE INFO

Article history:
Received 15 July 2021
Revised 24 September 2021
Accepted 2 October 2021
Available online 18 October 2021

Keywords:
Electrocatalysis
Materials screening
Volcano plot
Activity descriptor
Surface charging relation
Potential of zero charge

ABSTRACT

The generic volcano plot is a widely employed practical tool to display and compare the activity of different electrocatalysts in dependence of a small number of descriptors. It is known that the apex of the volcano curve shifts with applied potential. However, the trend of the potential-dependent shift of the volcano apex has remained unclear. Herein, we address this question for a two-step electrocatalytic reaction. With the transfer coefficient assumed as 1/2, our analysis reveals that the adsorbate coverage at the volcano apex equals 1/2 regardless of potential. We present a criterion to predict the direction and magnitude of the apex shift as a function of the activation energies of the two steps. Thereafter, the criterion is extended to the oxygen reduction reaction. The influence of the transfer coefficient and the potential of zero charge on the volcano plot is revealed. Implications of the presented criterion for targeted design of electrocatalysts are discussed.

1. INTRODUCTION

Electrocatalyst materials are needed in electrochemical devices to accelerate vital reactions, such as the oxygen reduction or evolution reactions [1,2]. In this context, concepts founded on the Sabatier-volcano principle find increasing use in comparative analyses and materials screening [3–5]. In the archetypal variant, a volcano plot relates the activities of a class of catalytic materials to the chemisorption strength of reaction intermediates. In the 1950s, Parsons [6] and Gerischer [7] derived a volcano-shape curve for the hydrogen evolution reaction (HER). The curve is a manifestation of the Sabatier principle of heterogeneous catalysis [8], which states that the interaction between a catalyst surface and adsorbed reaction intermediates should be neither too strong nor too weak. In the 1970s, Trasatti compiled the first experiment-based volcano plot for the HER which employed the hydrogen adsorption enthalpy extracted earlier by Krishtalik from experimental data [9,10]. Platinum was found at a location closest to the apex of the volcano curve.

Stepping into the 21st century, quantum-chemistry calculations in tandem with the computational hydrogen electrode approach have enabled the generation of extensive databases of adsorption energies [11,12], shedding new light on the pertinent criteria for catalyst design. It has been claimed that, for the optimal electrocatalyst material, the equilibrium potential of each reaction step must be equal to the overall equilibrium potential [13]. In this vein, considering a two-step two-electron reaction, the binding energy of the reaction intermediate (RI) should be precisely half of the sum of the free energy of reactant and product states. If reaction is controlled at its overall equilibrium potential, then it features a perfectly flat free energy profile (in the sense that no activation free energy is considered). A material with the ideal energetic properties for the reaction of interest is called a thermodynamically neutral one [10].

This approach assesses the catalyst activity by the so-called thermodynamic limiting potential (U_L), the potential at which the reaction energy of the thermodynamically least favorable step approaches 0. In other words: once U_L is achieved, no step is uphill [14]. The relation between U_L and the intermediate binding energy translates into a thermodynamic volcano plot (TDVP). Owing to its simple concept and advances in *ab initio* techniques [15,16], computational materials screening based on the TDVP has made deep inroads into electrocatalysis [3,4].

The curse and the blessing of the TDVP both lie in its simplicity, that is, catalyst activity is solely determined by binding energies of adsorbed intermediates. Schmickler *et al.* suggested that a complete picture of catalyst activity for the HER should entail at least two more properties: the relative position of the metal d-band and the Fermi level, and the interaction strength between the d-band

* Corresponding author.
E-mail address: m.eikerling@fz-juelich.de (M. Eikerling).

https://doi.org/10.1016/j.electacta.2021.139413

and the hydrogen 1 s orbital [17]. Though not independent, these two factors as well as the binding energy sometimes act against each other, as discussed in ref 14. Besides, another severe limitation of the analysis based on the TDVP is that it ignores the impact of activation energies and applied overpotential.

A recent experimental study revealed that the assumption of thermoneutrality for the optimal catalyst in the TDVP analysis failed to explain the superior activity of RuO_2 over IrO_2 for the oxygen evolution reaction (OER) or the chlorine evolution reaction (CER) [18–20]. A kinetic volcano plot, compiled by Exner, explained this anomaly [21]. It exposes a shift of the volcano apex towards more weakly bound intermediates with increasing overpotential for both reduction and oxidation reactions. Instead of being controlled by U_L, the activity is controlled by the energy difference between the initial configuration of the surface (identified from the DFT-based Pourbaix diagram) and the highest transition state in the free energy diagram (FED) of the reaction [22–24], similar to the property considered in the energetic span model devised by Kozuch and Shaik [25,26] and introduced to the field of electrocatalysis by Chen et al. [27,28]. More recently, by microkinetic modeling, Zhang, Zhang and Huang pointed out that, for the oxygen reduction reaction (ORR), an increase in overpotential shifts the optimal catalyst (in terms of the turnover frequency, TOF) to stronger oxygen bonding [29]. Around the same time, Ooka and Namakura derived a potential-dependent volcano plot for the HER and demonstrated that the apex could shift in either direction depending on reaction conditions [30].

Until now, the deviation of the optimal material from the prediction based on the TDVP has been reported for many crucial reactions (HER, ORR, CER, to name a few) [19,21,29,30]. It could be rationalized by the potential dependence of the volcano plot [29,30]. Nevertheless, there is a lack of a universal criterion to determine, for any given reaction, in which direction the kinetic volcano apex shifts. In order to predict the optimal material at any overpotential, it is a pressing need to provide such a criterion.

For a two-step reaction with one adsorbed intermediate, the adsorbate binding energy is the descriptor of a conventional one-dimensional volcano plot. A multi-step reaction with n (n>2) types of adsorbed intermediates requires an n-dimensional volcano plot which, by employing scaling relations, can be reduced to a one-dimensional one in the most expedient case [14]. However, in addition to the binding energy, surface charging relations and local conditions at the reaction plane severely alter the catalyst activity [31–35]. Thus, a volcano plot considering these effects would be suitable for a meaningful comparison of different catalysts. On the one hand, catalyst-specific parameters, such as transfer coefficient α and the potential of zero charge (PZC) ϕ_{PZC}, add extra dimensions to volcano plots [36]. On the other hand, catalyst-nonspecific parameters, such as reactant concentrations and electrode potential, will affect the shape and peak position of volcano plots.

In this article, we analyze a two-step proton-coupled electron transfer (PCET) reaction to understand the parametric effects that control the peak shift. We first prove that, on the premise of the transfer coefficient being 1/2, the optimal catalyst at any given potential is the one that exhibits half coverage by adsorbed intermediates. Then, we provide a criterion that pinpoints the shift direction of the volcano apex. This criterion focuses on the effect of changes in activation energies while other kinetic factors are assumed constant to retain a low-dimensional volcano plot. After generalizing the criterion with respect to reactant and product concentrations, we demonstrate its applicability to ORR, a multi-step PCET reaction. Following that analysis, systematic studies on the influence of the surface charging relations and intrinsic kinetic parameters on the criterion are carried out. A discussion of implications for materials screening and design concludes this contribution.

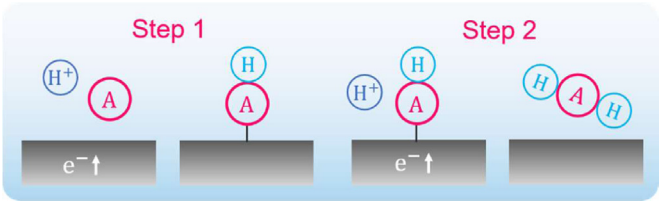

Scheme 1. Schematic of the two-step PCET reaction. In the first step, reactant A receives an electron and a proton, forming a chemisorbed intermediate AH. In the second step, AH receives another electron-proton pair, transforms into AH_2 and desorbs from the electrode surface.

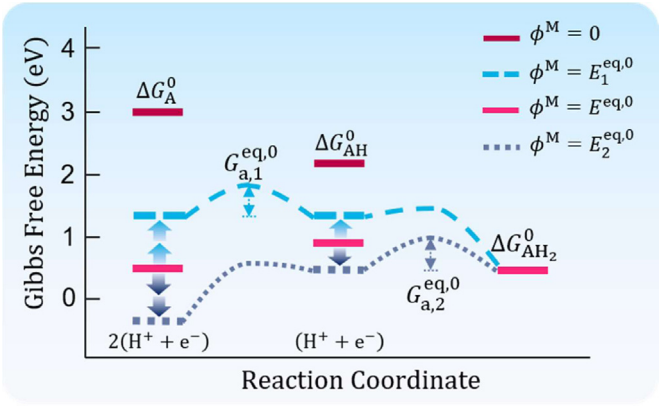

Scheme 2. Free energy diagram illustrating the base-case parameters. The conventional computational hydrogen electrode scheme is used here [14]. The superscript "eq" in $G_{a,1}^{eq,0}$ (or $G_{a,2}^{eq,0}$) denotes that step 1 (or step 2) is in equilibrium when the activation energy is measured.

2. MODEL DEVELOPMENT

2.1. Reaction scheme

The considered two-step proton-coupled electron transfer reaction is

$$* + \mathbf{A} + \mathbf{e}^- + \mathbf{H}^+ \leftrightarrow \mathbf{AH}^* \tag{1a}$$

$$\mathbf{AH}^* + \mathbf{e}^- + \mathbf{H}^+ \leftrightarrow \mathbf{AH}_2 + * \tag{1b}$$

As illustrated in **Scheme 1**, in step 1, A is chemisorbed onto the catalyst surface to form an intermediate AH*. In step 2, the intermediate is desorbed after receiving an electron and a proton. This two-step reaction scheme applies directly for several important reactions, for example, with AH* being H* for the HER ($2H^+ + 2e^- \rightarrow H_2$) or being COOH* for the CO_2 reduction reaction at Au or Ag surfaces ($CO_2 + 2H^+ + 2e^- \rightarrow CO + H_2O$).

2.2. Microkinetic model

The reaction equations are

$$v_1 = k_1[\mathbf{H}^+][\mathbf{A}](1 - \theta_{\mathbf{AH}}) - k_{-1}\theta_{\mathbf{AH}} \tag{2a}$$

$$v_2 = k_2[\mathbf{H}^+]\theta_{\mathbf{AH}} - k_{-2}[\mathbf{AH}_2](1 - \theta_{\mathbf{AH}}) \tag{2b}$$

where k_i and k_{-i} are the forward and backward rate constants of step i, and θ_{AH} is the coverage of AH*. Definitions and values of base-case parameters are given in **Table 1** and shown in **Scheme 2**. Particularly, ΔG_{AH}^0 does not affect $G_{a,1}^{eq,0}$ or $G_{a,2}^{eq,0}$, as the Bronsted–Evans–Polanyi relation can be written as $G_{a,i}^0 = G_{a,i}^{eq,0} + \alpha \Delta G_{r,i}^0$ with $\Delta G_{r,i}^0$ being the reaction free energy of step i [37]. Moreover, the

Table 1
Base-case parameters.

Symbol	Definition	Value
$[\mathbf{A}]$	Dimensionless concentration of A	1
$[\mathbf{AH_2}]$	Dimensionless concentration of AH_2	1
$[\mathbf{H^+}]_\mathbf{b}$	Dimensionless concentration of H^+ in the bulk solution	1
$\boldsymbol{\alpha}$	Transfer coefficient of step 1 and 2	0.5
$\Delta \boldsymbol{G}^0_\mathbf{A}$	Standard[a] Gibbs energy of A	3 eV
$\Delta \boldsymbol{G}^0_{\mathbf{AH_2}}$	Standard Gibbs energy of AH_2	0.5 eV
$\boldsymbol{E}_1^{\mathbf{eq},0}$	Standard equilibrium potential of step 1	$(\Delta G^0_\mathrm{A} - \Delta G^0_\mathrm{AH})/e$
$\boldsymbol{E}_2^{\mathbf{eq},0}$	Standard equilibrium potential of step 2	$(\Delta G^0_\mathrm{AH} - \Delta G^0_{\mathrm{AH_2}})/e$
$\boldsymbol{G}_{\mathbf{a},1}^{\mathbf{eq},0}$	Standard activation energy of the first step at $E_1^{\mathrm{eq},0}$	0.5 eV
$\boldsymbol{G}_{\mathbf{a},2}^{\mathbf{eq},0}$	Standard activation energy of the second step at $E_2^{\mathrm{eq},0}$	0.5 eV
$\varepsilon_\mathbf{w}$	Permittivity of water	$78.5\varepsilon_0$

[a] Standard state corresponds to 298 K, 1 bar, 0 V applied potential vs the standard hydrogen electrode (SHE), 1 mol/L concentration for soluble reactants and 1 bar pressure for gaseous reactants.

values of ΔG^0_A and $\Delta G^0_{\mathrm{AH_2}}$ are selected to ensure the overall equilibrium potential, $E^{\mathrm{eq},0} = (\Delta G^0_\mathrm{A} - \Delta G^0_{\mathrm{AH_2}})/2e$, is around 1 V, which is a moderate value.

At steady state, we have

$$\boldsymbol{v}_1 = \boldsymbol{v}_2 = \mathbf{TOF} \tag{3}$$

where TOF is the turnover frequency. Substituting Eqs. (2) into Eq. (3) and solving for θ_{AH} gives

$$\boldsymbol{\theta}_{\mathbf{AH}} = \frac{\boldsymbol{k}_1[\mathbf{H^+}][\mathbf{A}] + \boldsymbol{k}_{-2}[\mathbf{AH_2}]}{\boldsymbol{k}_1[\mathbf{H^+}][\mathbf{A}] + \boldsymbol{k}_2[\mathbf{H^+}] + \boldsymbol{k}_{-1} + \boldsymbol{k}_{-2}[\mathbf{AH_2}]} \tag{4}$$

$$\mathbf{TOF} = \frac{\boldsymbol{k}_1\boldsymbol{k}_2[\mathbf{H^+}]^2[\mathbf{A}] - \boldsymbol{k}_{-1}\boldsymbol{k}_{-2}[\mathbf{AH_2}]}{\boldsymbol{k}_1[\mathbf{H^+}][\mathbf{A}] + \boldsymbol{k}_2[\mathbf{H^+}] + \boldsymbol{k}_{-1} + \boldsymbol{k}_{-2}[\mathbf{AH_2}]} \tag{5}$$

with rate constants,

$$\boldsymbol{k}_1 = \boldsymbol{k}_0 \exp\left(-\frac{\boldsymbol{G}_{\mathbf{a},1}^{\mathbf{eq},0} + \boldsymbol{\alpha e}\left(\phi^{\mathbf{M}} - \phi^{\mathbf{OHP}} - \boldsymbol{E}_1^{\mathbf{eq},0}\right)}{\boldsymbol{k}_\mathbf{B}\boldsymbol{T}}\right) \tag{6}$$

$$\boldsymbol{k}_{-1} = \boldsymbol{k}_0 \exp\left(-\frac{\boldsymbol{G}_{\mathbf{a},1}^{\mathbf{eq},0} - (1-\boldsymbol{\alpha})\boldsymbol{e}\left(\phi^{\mathbf{M}} - \phi^{\mathbf{OHP}} - \boldsymbol{E}_1^{\mathbf{eq},0}\right)}{\boldsymbol{k}_\mathbf{B}\boldsymbol{T}}\right) \tag{7}$$

$$\boldsymbol{k}_2 = \boldsymbol{k}_0 \exp\left(-\frac{\boldsymbol{G}_{\mathbf{a},2}^{\mathbf{eq},0} + \boldsymbol{\alpha e}\left(\phi^{\mathbf{M}} - \phi^{\mathbf{OHP}} - \boldsymbol{E}_2^{\mathbf{eq},0}\right)}{\boldsymbol{k}_\mathbf{B}\boldsymbol{T}}\right) \tag{8}$$

$$\boldsymbol{k}_{-2} = \boldsymbol{k}_0 \exp\left(-\frac{\boldsymbol{G}_{\mathbf{a},2}^{\mathbf{eq},0} - (1-\boldsymbol{\alpha})\boldsymbol{e}\left(\phi^{\mathbf{M}} - \phi^{\mathbf{OHP}} - \boldsymbol{E}_2^{\mathbf{eq},0}\right)}{\boldsymbol{k}_\mathbf{B}\boldsymbol{T}}\right) \tag{9}$$

where ϕ^{M} and ϕ^{OHP} are the potential in the metal electrode and that at the position of the outer Helmholtz plane (OHP), respectively. The proton concentration at the OHP is then

$$\left[\mathbf{H^+}\right] = \left[\mathbf{H^+}\right]_\mathbf{b} \exp\left(-\frac{\boldsymbol{e}\phi^{\mathbf{OHP}}}{\boldsymbol{k}_\mathbf{B}\boldsymbol{T}}\right) \tag{10}$$

In the Gouy-Chapman model [38,39], ϕ^{OHP} is calculated from

$$\phi^{\mathbf{OHP}} + \frac{\sqrt{8[\mathbf{H^+}]_\mathbf{b}\boldsymbol{c}_{\mathbf{H^+}}^{\mathbf{ref}}\boldsymbol{k}_\mathbf{B}\boldsymbol{N}_\mathbf{A}\boldsymbol{T}\varepsilon_\mathbf{w}}\sinh\left(\frac{\boldsymbol{e}\phi^{\mathbf{OHP}}}{2\boldsymbol{k}_\mathbf{B}\boldsymbol{T}}\right)}{\frac{\varepsilon^{\mathbf{OHP}}}{\delta^{\mathbf{OHP}}}} = \phi^{\mathbf{M}} - \phi^{\mathbf{PZC}} \tag{11}$$

where $c^{\mathrm{ref}}_{\mathrm{H^+}}$ is the reference H^+ concentration, ε_w is the permittivity of bulk water, $\phi^{\mathbf{PZC}}$ is the potential of zero charge (PZC), and $\varepsilon^{\mathrm{OHP}}$ and δ^{OHP} are the permittivity and thickness of the medium between the OHP and the metal electrode surface, respectively. It is worthwhile to note that by PZC we always imply the potential of zero free charge [49].

Different catalysts have different ΔG^0_{AH} and PZCs. When generating a volcano plot, one of the most important yet usually overlooked aspects is that α and $G^{\mathrm{eq},0}_{\mathrm{a,i}}$ $(i = 1, 2)$, just like ΔG^0_{AH} and PZCs, do not remain the same among different materials. Thus, every parameter will contribute a degree of freedom, and a kinetic volcano plot accounting for all the parameters should be multidimensional. However, aiming for a simplified picture and an analytical result, we make the following assumptions when presenting and proving the criterion in the next section:

1 The supporting electrolyte is highly concentrated so that ϕ^{OHP} can be approximated to be 0 V, i.e., equal to the potential in the bulk solution (the reference potential). In this vein, the PZC does not play a role in the volcano analysis;
2 For the whole class of materials, $\alpha = 1/2$ for both step 1 and 2;

The assumptions will be the basis for the mathematical derivation in the following section. In the Discussion section, however, we will relax these assumptions one at a time and analyze the influence of each parameter.

3. CRITERION AND PROOF

The optimal binding energy corresponding to the volcano apex is denoted as $\Delta G^{\mathrm{optim}}_{\mathrm{AH}}$ and the overpotential is defined as $\eta = E^{\mathrm{eq},0} - \phi^{\mathrm{M}}$. The criterion for finding the optimal electrocatalyst at any overpotential will be formulated by the following theorem, which will be rigorously proved shortly.

THEOREM 1. *Consider a two-step proton-coupled electron transfer reaction in solution with high supporting-electrolyte concentration, $\alpha = 1/2$ and $[\mathrm{A}] = [\mathrm{AH_2}]$.*

If $G^{\mathrm{eq},0}_{\mathrm{a},1} < G^{\mathrm{eq},0}_{\mathrm{a},2}$, then as η increases, $\Delta G^{\mathrm{optim}}_{\mathrm{AH}}$ becomes more positive, and levels off at very large η.

If $G^{\mathrm{eq},0}_{\mathrm{a},1} = G^{\mathrm{eq},0}_{\mathrm{a},2}$, then as η increases, $\Delta G^{\mathrm{optim}}_{\mathrm{AH}}$ remains the same.

If $G^{\mathrm{eq},0}_{\mathrm{a},1} > G^{\mathrm{eq},0}_{\mathrm{a},2}$, then as η increases, $\Delta G^{\mathrm{optim}}_{\mathrm{AH}}$ becomes more negative, and levels off at large η.

Theorem 1 provides a universal criterion for the direction of the shift of the volcano apex with increasing overpotential η. **Fig. 1**a demonstrates the volcano plot for the case with $G^{\mathrm{eq},0}_{\mathrm{a},1} < G^{\mathrm{eq},0}_{\mathrm{a},2}$. As the overpotential increases, the volcano curve shifts up, and its apex moves towards right, asymptotically approaching a limiting value. The change of $\Delta G^{\mathrm{optim}}_{\mathrm{AH}}$ with η is shown in **Fig. 1**b for all three cases listed in Theorem 1. For $G^{\mathrm{eq},0}_{\mathrm{a},1} = G^{\mathrm{eq},0}_{\mathrm{a},2}$, $\Delta G^{\mathrm{optim}}_{\mathrm{AH}}$ remains 1.75 eV which is the thermoneutral value given by $(\Delta G^0_\mathrm{A} + \Delta G^0_{\mathrm{AH_2}})/2$. $G^{\mathrm{eq},0}_{\mathrm{a},1} > G^{\mathrm{eq},0}_{\mathrm{a},2}$ induces an opposite trend compared with $G^{\mathrm{eq},0}_{\mathrm{a},1} < G^{\mathrm{eq},0}_{\mathrm{a},2}$.

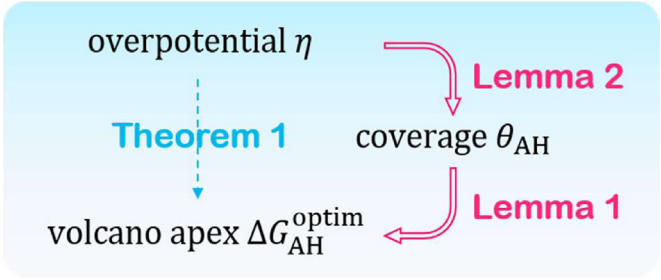

Scheme 3. Role of coverage θ_{AH} in the proof of Theorem 1: a link between ΔG_{AH}^{optim} and η. Using Lemma 1 and Lemma 2 with the help of θ_{AH} allowing for a much easier proof of Theorem 1.

Proving Theorem 1 directly by relating η with ΔG_{AH}^{optim} requires cumbersome mathematics. Instead, we will exploit θ_{AH} in an outflank strategy shown in **Scheme 3**. Lemma 1 will give the value of the optimal coverage, θ_{AH}^{optim}, corresponding to the volcano apex, while Lemma 2 will give the change of θ_{AH} with η. In short, θ_{AH} serves as a bridge which helps to locate the volcano apex at any overpotential.

LEMMA 1. *Consider a two-step proton-coupled electron transfer reaction in solution with high supporting-electrolyte concentration and* $\alpha = 1/2$. *Then, for any* η, $\theta_{AH}^{optim} = 1/2$.

Proof. We can find ΔG_{AH}^{optim} from the condition $d(TOF)/d(\Delta G_{AH}^0)|_{\Delta G_{AH}^{optim}} = 0$. Then, substituting the obtained ΔG_{AH}^{optim} into θ_{AH} gives the corresponding θ_{AH}^{optim}.

Here, as stated above, we assume $\phi^{OHP} = 0$. This assumption is valid for the case of a highly concentrated supporting electrolyte. Rewriting each term in the denominator of θ_{AH} in Eq. (4) (or that of TOF in Eq. (5)) as a function of ΔG_{AH}^0 yields

$$k_1[H^+][A] = k_0 \exp\left(-\frac{\alpha(\Delta G_{AH}^0 - \Delta G_A^0)}{k_B T}\right) \exp\left(-\frac{G_{a,1}^{eq,0} + \alpha e\phi^M}{k_B T}\right)[H^+][A] = A_1 \exp\left(-\frac{\alpha \Delta G_{AH}^0}{k_B T}\right) \quad (12)$$

$$k_2[H^+] = k_0 \exp\left(-\frac{\alpha(\Delta G_{AH_2}^0 - \Delta G_{AH}^0)}{k_B T}\right) \exp\left(-\frac{G_{a,2}^{eq,0} + \alpha e\phi^M}{k_B T}\right)[H^+] = B_1 \exp\left(\frac{\alpha \Delta G_{AH}^0}{k_B T}\right) \quad (13)$$

$$k_{-1} = k_0 \exp\left(\frac{(1-\alpha)(\Delta G_{AH}^0 - \Delta G_A^0)}{k_B T}\right) \exp\left(-\frac{G_{a,1}^{eq,0} - (1-\alpha) e\phi^M}{k_B T}\right) = C_1 \exp\left(\frac{(1-\alpha)\Delta G_{AH}^0}{k_B T}\right) \quad (14)$$

$$k_{-2}[AH_2] = k_0 \exp\left(\frac{(1-\alpha)(\Delta G_{AH_2}^0 - \Delta G_{AH}^0)}{k_B T}\right) \exp\left(-\frac{G_{a,2}^{eq,0} - (1-\alpha) e\phi^M}{k_B T}\right)[AH_2] = D_1 \exp\left(-\frac{(1-\alpha)\Delta G_{AH}^0}{k_B T}\right) \quad (15)$$

where A_1, B_1, C_1 and D_1 are independent of ΔG_{AH}^0 and given in the Supporting Information. By substituting Eqs. (12)-(15) to Eq. (4), we can express θ_{AH} as a function of ΔG_{AH}^0,

$$\theta_{AH} = \frac{A_1 \exp\left(-\frac{\Delta G_{AH}^0}{2k_B T}\right) + D_1 \exp\left(-\frac{\Delta G_{AH}^0}{2k_B T}\right)}{A_1 \exp\left(-\frac{\Delta G_{AH}^0}{2k_B T}\right) + B_1 \exp\left(\frac{\Delta G_{AH}^0}{2k_B T}\right) + C_1 \exp\left(\frac{\Delta G_{AH}^0}{2k_B T}\right) + D_1 \exp\left(-\frac{\Delta G_{AH}^0}{2k_B T}\right)}. \quad (16)$$

Meanwhile, the numerator of the TOF is expressed as

$$k_1 k_2 [H^+]^2 [A] - k_{-1} k_{-2} [AH_2] = A_1 B_1 - C_1 D_1, \quad (17)$$

which is independent of ΔG_{AH}^0. The reciprocal of TOF is then written as

$$TOF^{-1} \propto A_1 \exp\left(-\frac{\alpha \Delta G_{AH}^0}{k_B T}\right) + B_1 \exp\left(\frac{\alpha \Delta G_{AH}^0}{k_B T}\right) + C_1 \exp\left(\frac{(1-\alpha)\Delta G_{AH}^0}{k_B T}\right) + D_1 \exp\left(-\frac{(1-\alpha)\Delta G_{AH}^0}{k_B T}\right) \quad (18)$$

Taking the derivative, i.e., $d(TOF^{-1})/d(\Delta G_{AH}^0) = 0$, gives

$$\alpha A_1 \exp\left(-\frac{\alpha \Delta G_{AH}^0}{k_B T}\right) + (1-\alpha) D_1 \exp\left(-\frac{(1-\alpha)\Delta G_{AH}^0}{k_B T}\right) = \alpha B_1 \exp\left(\frac{\alpha \Delta G_{AH}^0}{k_B T}\right) + (1-\alpha) C_1 \exp\left(\frac{(1-\alpha)\Delta G_{AH}^0}{k_B T}\right) \quad (19)$$

With $\alpha = 1/2$ and substituting Eq. (16) to Eq. (19), we finally arrive at $\theta_{AH}^{optim} = 1/2$, which is also confirmed by numerical simulations of the volcano plot and θ_{AH} at four different values of η, as illustrated in **Fig. 2**. Note that the proof of Lemma 1 is independent of the values of [A] and [AH_2]. □

In the case of $\alpha = 1/2$, as considered here, the optimal binding energy is calculated by inserting $\theta_{AH} = 1/2$ into Eq. (16),

$$\Delta G_{AH}^{optim} = k_B T \ln \frac{A_1 + D_1}{B_1 + C_1} \quad (20)$$

where A_1, B_1, C_1 and D_1 are dependent on η (see the Supporting Information), so ΔG_{AH}^{optim} is a function of η. In the limit of high overpotential, when C_1 and D_1 can be neglected, we obtain

$$\Delta G_{AH}^{optim}|_{\eta\ high} = \frac{\Delta G_A^0 + \Delta G_{AH_2}^0}{2} + k_B T \ln[A] + G_{a,2}^{eq,0} - G_{a,1}^{eq,0} \quad (21)$$

The fact that $\Delta G_{AH}^{optim}|_{\eta\ high}$ is invariant with η corroborates the statement in Theorem 1: ΔG_{AH}^{optim} *levels off at large* η. The first term is the binding energy of the so-called thermoneutral catalyst at the equilibrium potential [12,13]. The second and last two terms account for the deviation from thermoneutrality because of concentration and activation energies. The larger the difference in activation energies, the larger the deviation of the optimal catalyst from the thermoneutral one; the deviation could be well above 0.2 eV, the uncertainty in binding energy from DFT calculations [40].

Having established that the optimal performance occurs at $\theta_{AH}^{optim} = 1/2$ (for $\alpha = 1/2$), the correlation between coverage and overpotential, which will be introduced by LEMMA 2, allows connecting the position of the volcano apex with the overpotential (see **Scheme 3**).

LEMMA 2. *Consider a two-step proton-coupled electron transfer reaction in solution with high supporting-electrolyte concentration,* $\alpha = 1/2$ *and* [A] = [AH_2].

If $G_{a,1}^{eq,0} < G_{a,2}^{eq,0}$, *then for any catalyst, as* η *increases,* θ_{AH} *increases.* i.e., $d\theta_{AH}/d\eta > 0$.

If $G_{a,1}^{eq,0} = G_{a,2}^{eq,0}$, *then for any catalyst, as* η *increases,* θ_{AH} *remains the same.*

If $G_{a,1}^{eq,0} > G_{a,2}^{eq,0}$, *then for any catalyst, as* η *increases,* θ_{AH} *decreases.* i.e., $d\theta_{AH}/d\eta < 0$.

Proof. Rewriting each term in θ_{AH} as a function of $\tilde{\eta} = \frac{e\eta}{k_B T}$,

$$k_1[H^+][A] = k_0 \exp\left(-\frac{\Delta G_{AH}^0 - \Delta G_A^0}{2k_B T}\right) \exp\left(-\frac{G_{a,1}^{eq,0} + 0.5 e\phi^M}{k_B T}\right)[H^+][A] = A_2 \exp(0.5\tilde{\eta}) \quad (22)$$

$$k_2[H^+] = k_0 \exp\left(-\frac{\Delta G_{AH_2}^0 - \Delta G_{AH}^0}{2k_B T}\right) \exp\left(-\frac{G_{a,2}^{eq,0} + 0.5 e\phi^M}{k_B T}\right)[H^+]$$

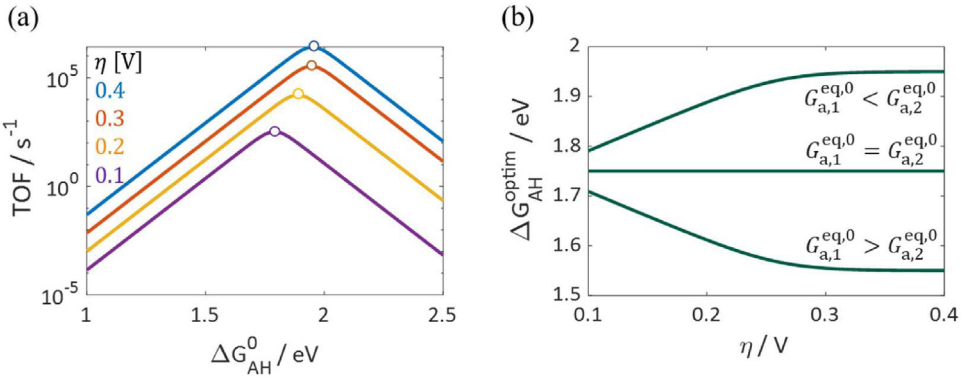

Fig. 1. Illustration of Theorem 1. a) Kinetic volcano plot at four different overpotential ηs assuming $G_{a,1}^{eq,0} = 0.4$ eV and $G_{a,2}^{eq,0} = 0.6$ eV. The volcano apex moves to the right with increasing η; b) The optimal binding energy as a function of η for $G_{a,1}^{eq,0} = 0.4$ eV, $G_{a,2}^{eq,0} = 0.6$ eV; $G_{a,1}^{eq,0} = 0.5$ eV, $G_{a,2}^{eq,0} = 0.5$ eV; $G_{a,1}^{eq,0} = 0.6$ eV, $G_{a,2}^{eq,0} = 0.4$ eV. The trends are in line with that stated in Theorem 1. For both a) and b), parameters other than $G_{a,i}^{eq,0}$ retain their base values shown in Table 1.

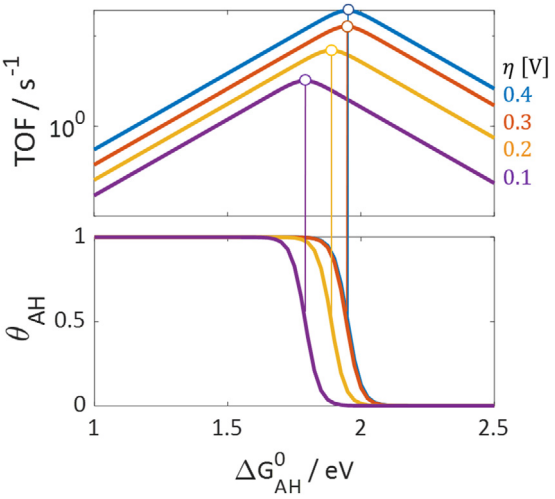

Fig. 2. The upper subfigure is the volcano plot for $G_{a,1}^{eq,0} = 0.4$ eV and $G_{a,2}^{eq,0} = 0.6$ eV at different values of the overpotential η. Other parameters retain their base values in Table . The lower subfigure shows θ_{AH} as a function of ΔG_{AH}^0. Changing overpotential does not alter $\theta_{AH}^{optim} = 1/2$.

$$= \boldsymbol{B}_2 \exp(0.5\tilde{\boldsymbol{\eta}}) \tag{23}$$

$$\boldsymbol{k}_{-1} = \boldsymbol{k}_0 \exp\left(\frac{\Delta \boldsymbol{G}_{AH}^0 - \Delta \boldsymbol{G}_A^0}{2\boldsymbol{k}_B \boldsymbol{T}}\right) \exp\left(-\frac{\boldsymbol{G}_{a,1}^{eq,0} - 0.5\boldsymbol{e}\phi^M}{\boldsymbol{k}_B \boldsymbol{T}}\right) = \boldsymbol{C}_2 \exp(-0.5\tilde{\boldsymbol{\eta}}) \tag{24}$$

$$\boldsymbol{k}_{-2}[\mathbf{AH}_2] = \boldsymbol{k}_0 \exp\left(\frac{\Delta \boldsymbol{G}_{AH_2}^0 - \Delta \boldsymbol{G}_{AH}^0}{2\boldsymbol{k}_B \boldsymbol{T}}\right) \exp\left(-\frac{\boldsymbol{G}_{a,2}^{eq,0} - 0.5\boldsymbol{e}\phi^M}{\boldsymbol{k}_B \boldsymbol{T}}\right)[\mathbf{AH}_2]$$
$$= \boldsymbol{D}_2 \exp(-0.5\tilde{\boldsymbol{\eta}}) \tag{25}$$

gives,

$$\boldsymbol{\theta}_{AH} = \frac{\boldsymbol{A}_2 \exp(0.5\tilde{\boldsymbol{\eta}}) + \boldsymbol{D}_2 \exp(-0.5\tilde{\boldsymbol{\eta}})}{\boldsymbol{A}_2 \exp(0.5\tilde{\boldsymbol{\eta}}) + \boldsymbol{B}_2 \exp(0.5\tilde{\boldsymbol{\eta}}) + \boldsymbol{C}_2 \exp(-0.5\tilde{\boldsymbol{\eta}}) + \boldsymbol{D}_2 \exp(-0.5\tilde{\boldsymbol{\eta}})} \tag{26}$$

where A_2, B_2, C_2 and D_2 are independent of $\tilde{\eta}$, and given in the Supporting Information. Taking the derivative of θ_{AH} with respect to $\tilde{\eta}$ gives

$$\frac{\mathrm{d}\boldsymbol{\theta}_{AH}}{\mathrm{d}\tilde{\boldsymbol{\eta}}} = \frac{\boldsymbol{A}_2\boldsymbol{C}_2 - \boldsymbol{B}_2\boldsymbol{D}_2}{(\boldsymbol{A}_2 \exp(0.5\tilde{\boldsymbol{\eta}}) + \boldsymbol{B}_2 \exp(0.5\tilde{\boldsymbol{\eta}}) + \boldsymbol{C}_2 \exp(-0.5\tilde{\boldsymbol{\eta}}) + \boldsymbol{D}_2 \exp(-0.5\tilde{\boldsymbol{\eta}}))^2} \tag{27}$$

$\frac{\mathrm{d}\theta_{AH}}{\mathrm{d}\tilde{\eta}} > 0$ warrants $A_2C_2 > B_2D_2$, which can be written as

$$\boldsymbol{G}_{a,1}^{eq,0} - \frac{1}{2}\boldsymbol{k}_B\boldsymbol{T}\ln[\mathbf{A}] < \boldsymbol{G}_{a,2}^{eq,0} - \frac{1}{2}\boldsymbol{k}_B\boldsymbol{T}\ln[\mathbf{AH}_2] \tag{28}$$

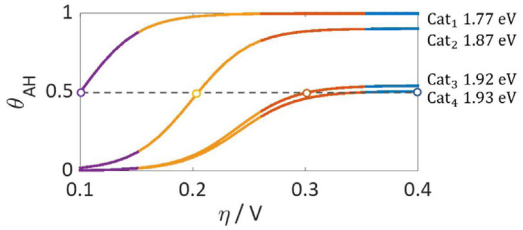

Fig. 3. The coverage of the adsorbed intermediate θ_{AH} as a function of overpotential η for four different catalysts Cat_1~Cat_4 for the case with $G_{a,1}^{eq,0} = 0.4$ eV and $G_{a,2}^{eq,0} = 0.6$ eV. Binding energies of the four catalysts are showed in the plot. The curves are divided into four overpotential regimes, within which the color is the same as that used in Fig. 2. Other parameters retain their base values in Table 1.

Because of $[A] = [AH_2]$, the condition is $G_{a,1}^{eq,0} < G_{a,2}^{eq,0}$. In the same vein, $\frac{\mathrm{d}\theta_{AH}}{\mathrm{d}\tilde{\eta}} = 0$ requires $G_{a,1}^{eq,0} = G_{a,2}^{eq,0}$ and $\frac{\mathrm{d}\theta_{AH}}{\mathrm{d}\tilde{\eta}} < 0$ requires $G_{a,1}^{eq,0} > G_{a,2}^{eq,0}$. □

Proof. *of Theorem 1.*

Let's consider the case with $G_{a,1}^{eq,0} < G_{a,2}^{eq,0}$. The other two cases follow the same logic. It is proved by Lemma 1 that the optimal catalyst is half-covered by the adsorbed intermediate irrespective of η. Therefore, the optimal catalyst denoted by Cat_1 at a certain overpotential η_1 is half-covered. As the overpotential increases to η_2, Lemma 2 implies that θ_{AH} of Cat_1 increases above 1/2, shifting it away from the volcano apex. Therefore, the optimal catalyst at η_2 should bind AH* weaker than Cat_1 to ensure that the "half-coverage" requirement is fulfilled. Equivalently speaking, as overpotential increases from η_1 to η_2, ΔG_{AH}^{optim} becomes more positive.

At sufficiently high η, we have

$$\theta_{AH} = \frac{A_2 \exp(\tilde{\eta}/2) + D_2 \exp(-\tilde{\eta}/2)}{A_2 \exp(\tilde{\eta}/2) + B_2 \exp(\tilde{\eta}/2) + C_2 \exp(-\tilde{\eta}/2) + D_2 \exp(-\tilde{\eta}/2)}$$

$$\approx \frac{\boldsymbol{A}_2 \exp\left(\frac{\tilde{\eta}}{2}\right)}{\boldsymbol{A}_2 \exp\left(\frac{\tilde{\eta}}{2}\right) + \boldsymbol{B}_2 \exp\left(\frac{\tilde{\eta}}{2}\right)} = \frac{\boldsymbol{A}_2}{\boldsymbol{A}_2 + \boldsymbol{B}_2}. \tag{29}$$

Because A_2 and B_2 are independent of η (see the Supporting Information), θ_{AH} becomes independent of η in this limit, so that ΔG_{AH}^{optim} levels off. □

We will use a concrete example to illustrate the proof. We assume $G_{a,1}^{eq,0} = 0.4$eV and $G_{a,2}^{eq,0} = 0.6$eV, while the other parameters are set at the base values in Table . θ_{AH} as a function of η is plotted in **Fig. 3** for four different catalysts, Cat_1 to Cat_4, with increasing binding energies.

At $\eta = 0.1$V, Lemma 1 tells us that the best catalyst is Cat_1 with 50% coverage and features a binding energy of 1.77 eV. As η increases to 0.2V, the coverage on Cat_1 increases to almost 100%, which is in line with Lemma 2. However, only by reducing the coverage to 50% can the optimal catalytic activity be achieved. Thus at $\eta = 0.2$V, catalyst Cat_2, with weaker bond strength (more positive binding energy), is half-covered by AH, and hence standing at the volcano apex. As $\eta > 0.3$V, θ_{AH} is almost invariant with η, so the change of ΔG_{AH}^{optim} is negligible.

4. DISCUSSION

4.1. Generalization to the case with $[A] \neq [AH_2]$

In most real situations, the dimensionless concentrations of the reactant and product are different. Without the assumption of $[A] = [AH_2]$, the condition $G_{a,1}^{eq,0} < G_{a,2}^{eq,0}$ in Theorem 1 will change to $G_{a,1}^{eq,0} - \frac{1}{2}k_BT\ln[A] < G_{a,2}^{eq,0} - \frac{1}{2}k_BT\ln[AH_2]$ according to Equation (28).

Recalling $E^{eq} = -\frac{\Delta G_r}{ne}$ and the Nernst equation $E^{eq} = E^{eq,0} - \frac{k_BT}{ne}\ln\frac{[AH_2]}{[A]}$, the new condition to replace $G_{a,1}{}^{eq,0} < G_{a,2}{}^{eq,0}$ can be rewritten as

$$\Delta \boldsymbol{G}_{\mathbf{a}}^{\mathbf{eq},0} > \frac{1}{2}\Delta\Delta \boldsymbol{G}_{\mathbf{r}} \tag{30}$$

with $\Delta G_a^{eq,0} = G_{a,2}^{eq,0} - G_{a,1}^{eq,0}$ and $\Delta\Delta G_r = \Delta G_r - \Delta G_r^0 = -2e(E^{eq} - E^{eq,0})$.

4.2. Application to the ORR: a four-electron PCET reaction

The developed criterion can be used in the analysis of other electrocatalytic reactions that involve more steps and several intermediates, as will be demonstrated for the ORR in this section. The definition of $\Delta G_a^{eq,0}$ needs to be modified for multi-step reactions: $\Delta G_a^{eq,0} = G_{a,de}^{eq,0} - G_{a,ad}^{eq,0}$. Herein, the subscript 'ad' stands for the adsorption of reactant onto the catalyst surface (the first step), while 'de' stands for the desorption of the product from the catalyst surface (the last step).

The ORR pathway is given by Equation (31) [31],

$$* + \mathbf{O_2} + \mathbf{H^+} + \mathbf{e^-} \leftrightarrow \mathbf{OOH^*} \tag{31a}$$

$$* + \mathbf{OOH^*} \leftrightarrow \mathbf{OH^*} + \mathbf{O^*} \tag{33b}$$

$$\mathbf{O^*} + \mathbf{H^+} + \mathbf{e^-} \leftrightarrow \mathbf{OH^*} \tag{33c}$$

$$\mathbf{OH^*} + \mathbf{H^+} + \mathbf{e^-} \leftrightarrow \mathbf{H_2O} + * \tag{33d}$$

The microkinetic model is the same as that used in Ref. 25 and given in the Supporting Information. Here, we use $[O_2] = 0.032$, $[H_2O] = 1$, $G_{a,ad}^{eq,0} = G_{a,1}^{eq,0} = 0.37$eV, and $G_{a,de}^{eq,0} = G_{a,4}^{eq,0} = 0.26$eV. Simple calculation shows that $\Delta G_a^{eq,0} < \Delta\Delta G_r/2$ is fulfilled, which predicts that as η increases, the apex of the volcano plot will shift to stronger binding regime, and level off at large η.

Fig. 4 shows the volcano plot derived by the microkinetic model. As η increases, ΔG_{AH}^{optim} decreases, and levels off for $\eta >$ 0.53V. The generalized criterion predicts this behavior successfully.

4.3. Influence of kinetic parameters

In the above analyses, the criterion for the shift of the volcano apex has been proven and tested for the ORR with several restrictive assumptions on kinetic parameters. In this section, these assumptions are relaxed one at a time. We analyze the stability of the criterion against these variations. These tests are done for the generic two-step mechanism in Eqs. (1).

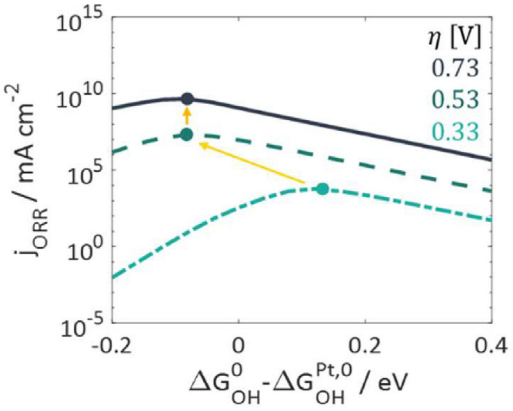

Fig. 4. Kinetic volcano plot of the ORR. $[O_2] = 0.032$, $[H_2O] = 1$, $G_{a,ad}^{eq,0} = G_{a,1}^{eq,0} =$ 0.37 eV, and $G_{a,de}^{eq,0} = G_{a,4}^{eq,0} = 0.26$ eV. Other parameters are the same as those used in Ref. 25. The condition, $\Delta G_a^{eq,0} > \Delta\Delta G_r/2$, is fulfilled. As η increases, the volcano apex moves to the left, and levels off at high η, as predicted by the generalized criterion.

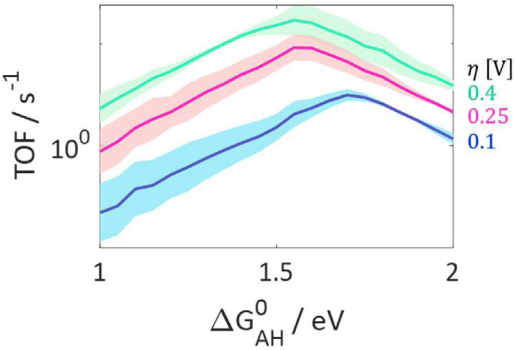

Fig. 5. Volcano curves of mean (deep-colored thin curve) and standard deviation (light-colored broad band) of 50 sets of TOF values. For each ΔG_{AH}^0, 50 sets of $[\alpha_1, \alpha_2]$ for step 1 and step 2 are used to generate the TOF values. $G_{a,1}^{eq,0} = 0.6$eV and $G_{a,2}^{eq,0} = 0.4$eV, and other parameters retain their base values. The overall trend of the apex shift remains the same as the criterion: for the case with $\Delta G_a^{eq,0} < \frac{1}{2}\Delta\Delta G_r$, ΔG_{AH}^{optim} becomes more negative, and levels off at large η.

4.4. Influence of transfer coefficient α

The transfer coefficient α may depart from 1/2 and differ among different steps for a single material as well as among different materials for a single step. Following the literature, typical values of α estimated theoretically lie in the range between 0.3 and 0.7 [22,33,41–44]. In this section, we study a group of 21 materials with the binding energy ΔG_{AH}^0 ranging from 1 to 2 eV in a step of 0.05 eV. Given that experimental data of α are scarce, we do not know the precise value of α for a given catalyst and a given step. Therefore, for each one of these materials we randomly assign 50 sets of $[\alpha_1, \alpha_2]$ between 0.3 and 0.7, as transfer coefficients of step 1 and step 2, respectively, and calculate the TOF. In this way, 50 different TOFs are obtained for every ΔG_{AH}^0. The mean and standard deviation of those TOFs, then, translate into the volcano plot shown in **Fig. 5**. Here, the condition $\Delta G_a^{eq,0} < \frac{1}{2}\Delta\Delta G_r$ is fulfilled by assuming $G_{a,1}^{eq,0} = 0.6$eV and $G_{a,2}^{eq,0} = 0.4$eV while other parameters retain their base values. The overall trend of the apex shift is preserved: as η increases, ΔG_{AH}^{optim} becomes more negative, and levels off at large η.

Table 2
PZCs of common catalysts. Here, the PZC refers to the potential of zero free charge. The electrolyte solution used for PZC tests is 0.1 M H_2SO_4. Data are collected from Ref. [46–49].

Metal	Ag(111)	Pt(100)	Pd(111)	Pt(111)	Au(111)	Ir(111)	Ru(111)
PZC / V_{SHE}	−0.50	0.34	0.21	0.29	0.47	0.02	0.06

4.5. Influence of ϕ^{OHP} and ϕ^{PZC}

Proper consideration of surface charging relations is indispensable when modeling electrocatalytic reactions [29,31,32,45]. The resulting local conditions at the reaction plane, such as ϕ^{OHP}, determines both the driving force of the reaction and the concentration of charged species (see Eq. (6)-(10)). For highly concentrated solutions, ions effectively screen the electric field, so ϕ^{OHP} can be approximated as 0 V relative to the potential in bulk solution. For less concentrated solutions, however, ϕ^{OHP} needs to be explicitly calculated. Employing Eq. (11), the case of $\phi^{M} > \phi^{PZC}$ gives $\phi^{OHP} > 0$. The assumption of $\phi_{OHP\,=\,0}$ leads to an underestimation of the driving force (Eq. (6) and (8)) and an overestimation of the proton concentration at the OHP (Eq. (10)). Because the influence of concentration is larger, the TOF will be overrated.

If PZCs are the same for the whole class of materials, so will be ϕ^{OHP} (assuming the reaction takes place in the same solution). In this vein, discarding the assumption of high solution concentration will only lead to a decrease in magnitude of the TOF curves, compared with the curves in **Fig. 1a**, while maintaining the trend for the apex shift, as stated in Theorem 1.

However, the difference in PZCs would result in different ϕ^{OHP}. In order to evaluate its effect, we employed PZC as another dimension to generate a two-dimensional volcano plot, and check if a certain set of PZCs alters the trend in ΔG_{AH}^{optim}. We evaluate the following two cases:

Case 1: overall equilibrium potential far from 0 V, here $E^{eq,0} = 1.25V$ is assumed; Case 2: overall equilibrium potential relatively close to 0 V, here $E^{eq,0} = 0.5V$ is assumed. For the following analyses in this section, we assume $G_{a,1}^{eq} = 0.6eV$ and $G_{a,2}^{eq} = 0.4eV$. Other parameters remain at their base values with the exception of $\Delta G_{AH_2}^{0}$ being 2eV for case 2 to impose $E^{eq,0} = 0.5V$.

Experimental values of the PZCs of common metal catalysts largely fall into the range between −0.5 V and 0.5 V, as listed in Table 2.[46–49] Thus, in the following analysis, the PZC axis varies in the range of [−0.5, 0.5].

Fig. 6 shows the volcano analyses for Case 1 (**Fig. 6**a,b) and Case 2 (c,d). Comparing the TOF of the class of materials with a certain value of the PZC, for example $\phi^{PZC,1}$ (the horizontal white solid lines in **Fig. 6**a), ΔG_{AH}^{optim} decreases with increasing overpotential. This is predicted by the criterion for reactions that fulfill $\Delta G_{a}^{eq,0} < \frac{1}{2}\Delta\Delta G_r$. Moreover, at a given overpotential, changing the PZCs of all materials by the same magnitude does not alter ΔG_{AH}^{optim}. This can be observed by the TOF values with $\phi^{PZC,1}$ and $\phi^{PZC,2}$, specified by the solid line and the dashed line in the upper subfigure of Fig. 6a.

For a certain binding energy, higher PZC leads to higher TOF, as can be seen in the longitudinal dotted line in **Fig. 6**c. The higher the PZC is, the lower ϕ^{OHP} would be (see Eq. (11)), which leads to a better performance. 1 V difference in the PZC could lead to 10 orders of magnitude difference in TOF (see **Fig. 6**c). As a catalyst-specific property, the PZC is likely to alter the activity trend predicted by previous thermodynamic and kinetic volcano plots in the literature that do not consider the PZC explicitly.

The influence of scattering PZCs of different catalysts is investigated in the following manner. For the first case, 21 materials with the binding energy ΔG_{AH}^{0} ranging from 1 to 2 eV with a step of 0.05 eV are studied. For case 2, another 21 materials from 2 to 3 eV are selected. In contrast to α, the PZC is a well-documented property of materials. Therefore, the "mean and standard deviation" treatment in the previous section is not necessary. Here, we intend to show how a volcano plot for a specific class of materials looks like. For each of these materials, a random value between −0.5 V and 0.5 V is assigned to the PZC (specified in the Supporting Information), then its TOF is calculated and compiled into a volcano plot (see Fig. 6b,d).

The fluctuation of the TOFs around the base-case volcano curves in Case 2 is larger than that of Case 1. Consequently, for a reaction with $E^{eq,0}$ close to 0 V, there could be several materials with up to 0.3 eV difference in ΔG_{AH}^{0} (marked by the full green circles) that exhibit very high activity in activity at high overpotential. At low overpotential, the optimal material (marked by the full blue circle) could deviate from the apex of the volcano curve by about 0.2 eV.

To sum up, the explicit consideration of the PZC exerts a larger influence on the criterion for reactions with $E^{eq,0}$ close to 0 V, such as the HER, than those with $E^{eq,0}$ far from 0 V, such as the ORR and the CO_2 reduction reaction.

4.6. Implications for materials screening

It is the common practice to evaluate catalysts in the low current density regime (~1 mA/cm^2), where mass transport effects do not affect the measured activity. However, as pointed out in this work, the sequence of catalyst activity as a function of a material descriptor that is obtained under these conditions could be misleading if used in real-world devices. For example, fuel cells operate at 0.6 to 0.9 V_{SHE} which is far from the equilibrium potential of the ORR. Recently devised experimental setups, such as that of Zalitis *et al.*, allow catalyst activities to be measured over a wide range of overpotentials without interference from mass transport effects [50,51]. In comparative analyses conducted at several high values of overpotential, the trend predicted by the presented criterion should be seen.

5. CONCLUSION

This contribution explores the origin of the overpotential-dependent volcano plot and provides a criterion that predicts whether the volcano apex shifts towards stronger or weaker binding direction with increasing overpotential. For the case of a generic two-step PCET reaction in highly concentrated solution with $\alpha = 1/2$ and $[A] = [AH_2]$, the shift direction of the apex depends on the relative magnitude of the two activation energies of the two reaction steps. At high overpotentials, the deviation of the optimal catalyst from the thermoneutral one can be larger than 0.2 eV, the uncertainties of DFT calculations [40].

The criterion is then generalized for cases without the assumption of $[A] = [AH_2]$ and proven effective for a multi-step reaction, *viz.* the ORR. Furthermore, kinetic parameters that are fixed in the derivation of Theorem 1, such as the transfer coefficient and the PZC, are then allowed to randomly fluctuate. With the transfer coefficient randomly sampled in the range between 0.3 and 0.7, the trend in the shift of the volcano apex remains valid. The scattering of the PZC between −0.5 and 0.5 V mainly affects the criterion when applying to reactions with the overall equilibrium potential close to 0 V (vs. the potential in bulk electrolyte solution); whereas

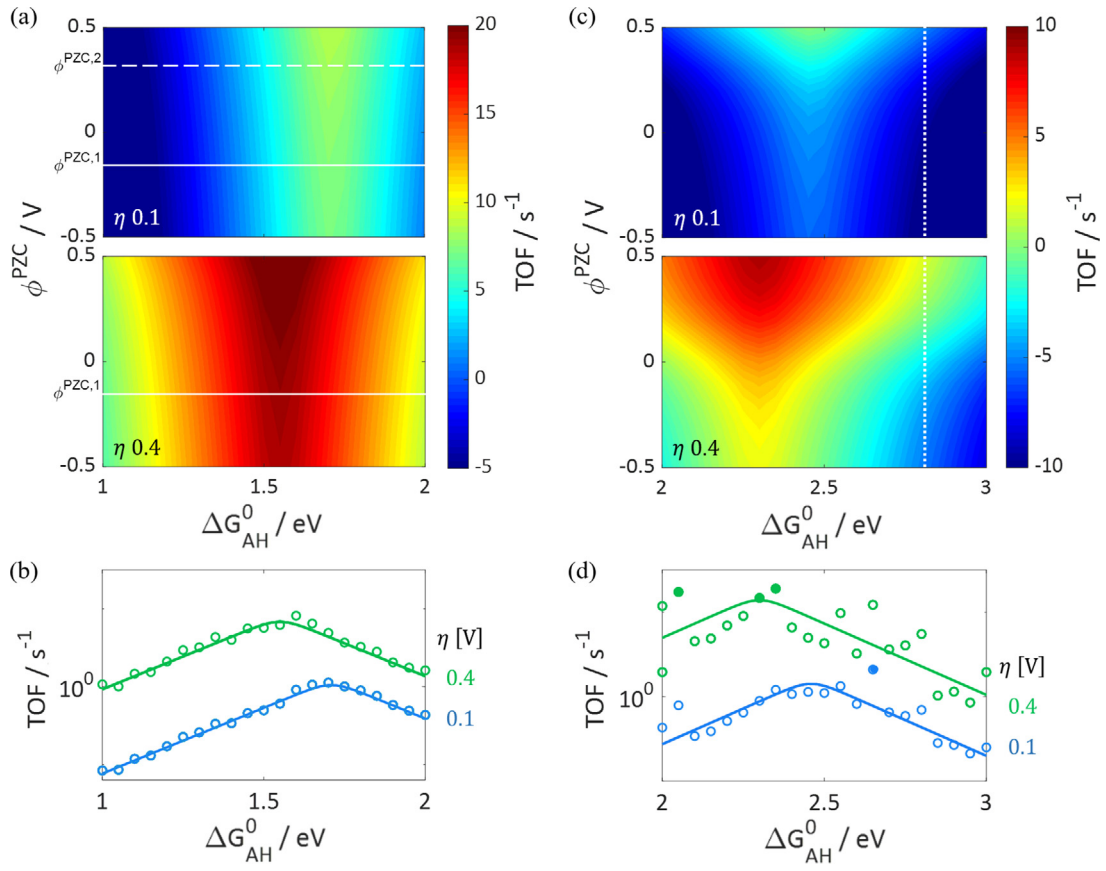

Fig. 6. (a), (c) Two-dimensional volcano plots for case 1 (a) and case 2 (c) at $\eta = 0.4$V and 0.1V. For a certain binding energy, higher ϕ^{PZC} leads to higher activity. Modifying the PZCs for the whole class of materials by the same magnitude does not shift ΔG_{AH}^{optim}. (b), (d) Volcano curves and TOF values at $\eta = 0.4$V and 0.1V for case 1 (b) and case 2 (d). Solid curves: volcano curves assuming $\phi^{PZC} = 0$V. Circles: TOF values obtained with a specific set of ϕ^{PZC}, randomly sampled from −0.5 to 0.5, for each material. The TOF values close to the highest activities at two different η are marked with full circles. The explicit consideration of the PZC exerts a higher impact on the criterion for case 2 than for case 1. For (a)∼(d), $G_{a,1}^{eq} = 0.6$eV, $G_{a,2}^{eq} = 0.4$eV, and other parameters retain their base values except $\Delta G_{AH}^{0} = 2$eV is assumed for (b) and (d).

reactions with $E^{eq,0}$ far from 0 V can be safely analyzed by the criterion.

The criterion would manifest itself in experiments when activities of a class of materials are tested from low to high overpotentials if mass transport losses are either eliminated or corrected for. The contribution emphasizes that comparative analyses of electrocatalyst materials should be considered as multiparameter problems. As demonstrated, especially the surface charging relation, which, in the simplest case, could be represented by the potential of zero charge, and intrinsic kinetic parameters of specific electron transfer processes, including the transfer coefficient, should be considered in descriptor-based approaches of catalyst screening.

Credit author statement

Yufan Zhang: Conceptualization, Methodology, Software, Validation, Visualization, Writing-Original Draft

Jun Huang: Conceptualization, Methodology, Writing - Review & Editing

Michael Eikerling: Conceptualization, Writing - Review & Editing, Supervision

Declaration of Competing Interest

The authors declare that they have no known competing financial interests or personal relationships that could have appeared to influence the work reported in this paper.

ACKNOWLEDGMENTS

ME acknowledges the financial support from Forschungszentrum Jülich GmbH. J.H. acknowledges the financial support from the Alexander von Humboldt Foundation and National Natural Science Foundation of China under the grant number of 21802170. Y.Z. gives special thanks to Xinwei Zhu at Forschungszentrum Jülich and Jinwen Liu at Changchun Institute of Applied Chemistry for critical discussions and valuable suggestions.

Supplementary materials

Supplementary material associated with this article can be found, in the online version, at doi:10.1016/j.electacta.2021.139413.

References

[1] , Introduction to Catalysis, in: Concepts of Modern Catalysis and Kinetics, John Wiley & Sons, Ltd, 2005, pp. 1–21, doi:10.1002/3527602658.ch1.
[2] I. Chorkendorff, J.W. Niemantsverdriet, Concepts of Modern Catalysis and Kinetics, 3rd Edition, Wiley-VCH, Weinheim, Deutschland, 2003.
[3] Z.W. Seh, J. Kibsgaard, C.F. Dickens, I. Chorkendorff, J.K. Nørskov, T.F. Jaramillo, Combining theory and experiment in electrocatalysis: insights into materials design, Science 355 (2017) eaad4998https://doi.org/, doi:10.1126/science.aad4998.
[4] M.M. Montemore, J.W. Medlin, Scaling relations between adsorption energies for computational screening and design of catalysts, Catal. Sci. Technol. 4 (2014) 3748–3761, doi:10.1039/C4CY00335G.
[5] J. Liu, H. Liu, H. Chen, X. Du, B. Zhang, Z. Hong, S. Sun, W. Wang, Progress and Challenges Toward the Rational Design of Oxygen Electrocatalysts Based on a Descriptor Approach, Adv. Sci. 7 (2020) 1901614, doi:10.1002/advs.201901614.

[6] R. Parsons, The rate of electrolytic hydrogen evolution and the heat of adsorption of hydrogen, Trans. Faraday Soc. 54 (1958) 1053–1063, doi:10.1039/TF9585401053.

[7] H. Gerischer, Mechanismus der Elektrolytischen Wasserstoffabscheidung und Adsorptionsenergie von Atomarem Wasserstoff, Bulletin des Sociétés Chimiques Belges 67 (1958) 506–527, doi:10.1002/bscb.19580670714.

[8] P. Sabatier, La Catalyse En Chimie organique, Librairie polytechnique, Paris et Liege, 1920.

[9] S. Trasatti, Work function, electronegativity, and electrochemical behaviour of metals: III. Electrolytic hydrogen evolution in acid solutions, J. Electroanal. Chem. Interfacial Electrochem. 39 (1972) 163–184, doi:10.1016/S0022-0728(72)80485-6.

[10] Paul. Delahay, C.W... Tobias, Advances in Electrochemistry and Electrochemical Engineering, 7, Interscience Publishers, New York; London; Sydney [etc.], 1970 Volume 7.

[11] J.K. Nørskov, J. Rossmeisl, A. Logadottir, L. Lindqvist, J.R. Kitchin, T. Bligaard, H. Jónsson, Origin of the Overpotential for Oxygen Reduction at a Fuel-Cell Cathode, J. Phys. Chem. B. 108 (2004) 17886–17892, doi:10.1021/jp047349j.

[12] J.K. Nørskov, T. Bligaard, A. Logadottir, J.R. Kitchin, J.G. Chen, S. Pandelov, U. Stimming, Trends in the Exchange Current for Hydrogen Evolution, J. Electrochem. Soc. 152 (2005) J23–J26, doi:10.1149/1.1856988.

[13] M.T.M. Koper, Theory of multiple proton–electron transfer reactions and its implications for electrocatalysis, Chem. Sci. 4 (2013) 2710–2723, doi:10.1039/C3SC50205H.

[14] A. Kulkarni, S. Siahrostami, A. Patel, J.K. Nørskov, Understanding Catalytic Activity Trends in the Oxygen Reduction Reaction, Chem. Rev. 118 (2018) 2302–2312, doi:10.1021/acs.chemrev.7b00488.

[15] K. Letchworth-Weaver, T.A. Arias, Joint density functional theory of the electrode-electrolyte interface: application to fixed electrode potentials, interfacial capacitances, and potentials of zero charge, Phys. Rev. B. 86 (2012) 075140, doi:10.1103/PhysRevB.86.075140.

[16] R. Sundararaman, W.A. Goddard, T.A. Arias, Grand canonical electronic density-functional theory: algorithms and applications to electrochemistry, J. Chem. Phys. 146 (2017) 114104, doi:10.1063/1.4978411.

[17] P. Quaino, F. Juarez, E. Santos, W. Schmickler, Volcano plots in hydrogen electrocatalysis – uses and abuses, Beilstein J. Nanotechnol. 5 (2014) 846–854, doi:10.3762/bjnano.5.96.

[18] D.-.Y. Kuo, H. Paik, J. Kloppenburg, B. Faeth, K.M. Shen, D.G. Schlom, G. Hautier, J. Suntivich, Measurements of Oxygen Electroadsorption Energies and Oxygen Evolution Reaction on RuO2(110): a Discussion of the Sabatier Principle and Its Role in Electrocatalysis, J. Am. Chem. Soc. 140 (2018) 17597–17605, doi:10.1021/jacs.8b09657.

[19] D.-.Y. Kuo, H. Paik, J.N. Nelson, K.M. Shen, D.G. Schlom, J. Suntivich, Chlorine evolution reaction electrocatalysis on RuO2(110) and IrO2(110) grown using molecular-beam epitaxy, J. Chem. Phys. 150 (2019) 041726, doi:10.1063/1.5051429.

[20] D. Zhou, J. Wei, Z.-.D. He, M.-.L. Xu, Y.-.X. Chen, J. Huang, Combining Single Crystal Experiments and Microkinetic Modeling in Disentangling Thermodynamic, Kinetic, and Double-Layer Factors Influencing Oxygen Reduction, J. Phys. Chem. C. 124 (2020) 13672–13678, doi:10.1021/acs.jpcc.0c01621.

[21] K.S. Exner, Beyond the Traditional Volcano Concept: overpotential-Dependent Volcano Plots Exemplified by the Chlorine Evolution Reaction over Transition-Metal Oxides, J. Phys. Chem. C. 123 (2019) 16921–16928, doi:10.1021/acs.jpcc.9b05364.

[22] K.S. Exner, I. Sohrabnejad-Eskan, H. Over, A Universal Approach To Determine the Free Energy Diagram of an Electrocatalytic Reaction, ACS Catal. 8 (2018) 1864–1879, doi:10.1021/acscatal.7b03142.

[23] K.S. Exner, Is Thermodynamics a Good Descriptor for the Activity? *Re*-Investigation of Sabatier's Principle by the Free Energy Diagram in Electrocatalysis, ACS Catal. 9 (2019) 5320–5329, doi:10.1021/acscatal.9b00732.

[24] K.S. Exner, Does a Thermoneutral Electrocatalyst Correspond to the Apex of a Volcano Plot for a Simple Two-Electron Process? Angew. Chem. Int. Ed. 59 (2020) 10236–10240, doi:10.1002/anie.202003688.

[25] S. Kozuch, S. Shaik, How to Conceptualize Catalytic Cycles? The Energetic Span Model, Acc. Chem. Res. 44 (2011) 101–110, doi:10.1021/ar1000956.

[26] E. Solel, N. Tarannam, S. Kozuch, Catalysis: energy is the measure of all things, Chem. Commun. 55 (2019) 5306–5322, doi:10.1039/C9CC00754G.

[27] J. Chen, Y. Chen, P. Li, Z. Wen, S. Chen, Energetic Span as a Rate-Determining Term for Electrocatalytic Volcanos, ACS Catal 8 (2018) 10590–10598, doi:10.1021/acscatal.8b03008.

[28] J. Li, Y. Ji, J. Chen, Z. Wen, Marking Electrocatalysts on the “Volcanic Belt” of Hydrogen Electrode Reactions, J. Phys. Chem. C. 125 (2021) 5587–5595, doi:10.1021/acs.jpcc.0c11115.

[29] Y. Zhang, J. Zhang, J. Huang, Potential-Dependent Volcano Plot for Oxygen Reduction: mathematical Origin and Implications for Catalyst Design, J. Phys. Chem. Lett. 10 (2019) 7037–7043, doi:10.1021/acs.jpclett.9b02436.

[30] H. Ooka, R. Nakamura, Shift of the Optimum Binding Energy at Higher Rates of Catalysis, J. Phys. Chem. Lett. 10 (2019) 6706–6713, doi:10.1021/acs.jpclett.9b01796.

[31] J. Huang, J. Zhang, M. Eikerling, Unifying theoretical framework for deciphering the oxygen reduction reaction on platinum, Phys. Chem. Chem. Phys. 20 (2018) 11776–11786, doi:10.1039/C8CP01315B.

[32] X. Zhu, J. Huang, Modeling Electrocatalytic Oxidation of Formic Acid at Platinum, J. Electrochem. Soc. 167 (2020) 013515, doi:10.1149/2.0152001JES.

[33] J. Huang, S. Chen, Interplay between Covalent and Noncovalent Interactions in Electrocatalysis, J. Phys. Chem. C. 122 (2018) 26910–26921, doi:10.1021/acs.jpcc.8b07534.

[34] S. Ringe, E.L. Clark, J. Resasco, A. Walton, B. Seger, A.T. Bell, K. Chan, Understanding cation effects in electrochemical CO2 reduction, Energy Environ. Sci. 12 (2019) 3001–3014, doi:10.1039/C9EE01341E.

[35] S. Ringe, C.G. Morales-Guio, L.D. Chen, M. Fields, T.F. Jaramillo, C. Hahn, K. Chan, Double layer charging driven carbon dioxide adsorption limits the rate of electrochemical carbon dioxide reduction on Gold, Nat. Commun. 11 (2020) 33, doi:10.1038/s41467-019-13777-z.

[36] K.S. Exner, Paradigm change in hydrogen electrocatalysis: the volcano's apex is located at weak bonding of the reaction intermediate, Int. J. Hydrog. Energy. 45 (2020) 27221–27229, doi:10.1016/j.ijhydene.2020.07.088.

[37] S. Wang, B. Temel, J. Shen, G. Jones, L.C. Grabow, F. Studt, T. Bligaard, F. Abild-Pedersen, C.H. Christensen, J.K. Nørskov, Universal Brønsted-Evans-Polanyi Relations for C–C, C–O, C–N, N–O, N–N, and O–O Dissociation Reactions, Catal. Lett. 141 (2011) 370–373, doi:10.1007/s10562-010-0477-y.

[38] M. Gouy, Sur la constitution de la charge électrique à la surface d'un électrolyte, J. Phys. Theor. Appl. 9 (1910) 457–468, doi:10.1051/jphystap:019100090045700.

[39] D.L. Chapman, LI, A contribution to the theory of electrocapillarity, London, Edinburgh Dublin Philos. Mag. J. Sci. 25 (1913) 475–481, doi:10.1080/14786440408634187.

[40] J. Wellendorff, T. Silbaugh, D. Pintos, J. Nørskov, T. Bligaard, F. Studt, C. Campbell, A benchmark database for adsorption bond energies to transition metal surfaces and comparison to selected DFT functionals, Surf. Sci. (2015) 640, doi:10.1016/j.susc.2015.03.023.

[41] C.H. Hamman, A. Hamnett, W. Vielstich, Electrochemistry, Wiley-VCH, Weinheim, 1997.

[42] J.O. Bockris, A.K.N. Ready, Modern Electrochemistry, Plenum Publishing Corporation, New York, 1973.

[43] R. Guidelli, R.G. Compton, J.M. Feliu, E. Gileadi, J. Lipkowski, W. Schmickler, S. Trasatti, Definition of the transfer coefficient in electrochemistry (IUPAC Recommendations 2014), Pure and Appl. Chem. 86 (2014) 259–262, doi:10.1515/pac-2014-5025.

[44] R.A. Marcus, Chemical and Electrochemical Electron-Transfer Theory, Annu. Rev. Phys. Chem. 15 (1964) 155–196, doi:10.1146/annurev.pc.15.100164.001103.

[45] L. Zhang, J. Huang, Understanding Surface Charge Effects in Electrocatalysis. Part I: peroxodisulfate Reduction at Pt(111), J. Phys. Chem. C. 124 (2020) 16951–16960, doi:10.1021/acs.jpcc.0c02824.

[46] S. Trasatti, E. Lust, The Potential of Zero Charge, in: R.E. White (Ed.), Modern Aspects of Electrochemistry, Springer, New York, 1999, pp. 1–215.

[47] S. Trasatti, Phenomenological Approach to Metal/Electrolyte Interfaces, Electrified Interfaces in Physics, Chemistry and Biology, Springer, Dordrecht, 1992.

[48] J. Le, M. Iannuzzi, A. Cuesta, J. Cheng, Determining Potentials of Zero Charge of Metal Electrodes versus the Standard Hydrogen Electrode from Density-Functional-Theory-Based Molecular Dynamics, Phys. Rev. Lett. 119 (2017) 016801, doi:10.1103/PhysRevLett.119.016801.

[49] O.A. Petrii, Zero charge potentials of platinum metals and electron work functions (Review), Russian J. Electrochem. 49 (2013) 401–422, doi:10.1134/S1023193513050145.

[50] C.M. Zalitis, D. Kramer, A.R. Kucernak, Electrocatalytic performance of fuel cell reactions at low catalyst loading and high mass transport, Phys. Chem. Chem. Phys. 15 (2013) 4329–4340, doi:10.1039/C3CP44431G.

[51] M. Markiewicz, C. Zalitis, A. Kucernak, Performance measurements and modelling of the ORR on fuel cell electrocatalysts – the modified double trap model, Electrochim. Acta. 179 (2015) 126–136, doi:10.1016/j.electacta.2015.04.066.